RSC Advances

ROYAL SOCIETY OF CHEMISTRY

www.rsc.org/advances

Tunable ternary (P, S, N)-doped graphene as an efficient electrocatalyst for oxygen reduction reaction in an alkaline medium

Yishu Wang, Bowen Zhang, Minghui Xu, Xingquan He*

Department of Chemistry and Chemical Engineering, Changchun University of Science and Technology, Changchun 130022, P. R. China.

*Corresponding author. Tel.+86-431-85583430
E-mail address:hexingquan@hotmail.com (Xingquan He)

Abstract

In this work, we utilize a one-step pyrolysis method to thermally synthesize phosphorus (P), sulfur (S) and nitrogen (N) ternary-doped graphene (PSNG) using graphene oxide (GO), phosphoric acid and thiourea precursors as a low-cost and high-efficient catalyst for the oxygen reduction reaction (ORR). The synthesized PSNG was characterized by transmission electron microscopy (TEM), X-ray diffraction (XRD), Raman spectroscopy, and X-ray photoelectron spectroscopy (XPS), respectively. The electrocatalytic activity of the PSNG composite towards ORR was evaluated by the linear sweep voltammetry (LSV) method. Electrochemical measurements reveal that the pyrolyzed PSNG at 1:10 mass ratio of phosphoric acid to thiourea has excellent catalytic activity towards ORR in an alkaline electrolyte, including large kinetic-limiting current density and good stability as well as a desirable four-electron pathway for the formation of water. These superior properties make the PSNG a kind of promising cathode catalyst for alkaline fuel cells.

Keywords: ternary-doped graphene; Pyrolysis; ORR; Fuels cells

1. Introduction

Electrochemical energy conversion and storage devices, ranging from fuel cells to metal–air batteries, demand high-efficient cathodic electrocatalysts for accelerating the sluggish oxygen reduction reaction (ORR) [1, 2]. It is well known, platinum (Pt) or Pt-based alloys have been regarded as the most active catalysts because they

provide the lowest overpotential and the highest current response towards a direct 4-electron reduction of oxygen to water [3]. However, the usage of electrocatalysts with high loading of Pt in the cathode, leads to high cost which hinders further commercialization [4,5]. Under these circumstances, seeking for novel, highly active, durable, and affordable non-precious-metal or metal-free electrocatalysts for ORR has been actively pursued over the past few decades [6-10].

Graphene, a unique two-dimensional monolayer structure of sp^2-hybridized carbon, has gained great attention in the fields of fuel cells, metal-air batteries and sensors because of its intriguing properties such as superior electrical conductivity, large surface area, excellent mechanical flexibility, and high thermal/chemical stability [11-15]. Furthermore, the some carbon atoms on the pristine graphene can be substituted by heteroatoms, such as N, B, P, S and F, the obtained heteroatom-doped graphene materials are considered to be effective electrocatalysts for ORR [16-22]. Although the details of all the mechanism that the heteroatoms improve the ORR electrocatalytic activities of doped carbons remain not yet well-understood, both theoretic calculation and experimental results indicate that substitution of C atoms with heteroatoms in the sp^2 lattice of graphitic carbon alters the electronic arrangement of carbon nano-materials (CNMs) and tailors their electron donor properties, and subsequently generates active sites for oxygen adsorption, thus leading to an improved ORR electrocatalytic activity [23-26].

At present, most studies are concentrated on dual-doped carbon materials such as N/F, N/B, N/P and N/S dual-doped CNMs, which displayed higher catalytic activity

than mono-doped carbon nano-materials. It is generally believed that dual-doping could not only provide more defective sites but also interact with each other to provide synergetic coupling effect, thus enhancing the ORR activity [18,19,21,22]. Besides the work focused on the binary doping of heteroatoms into the carbon structure, the ternary-doped carbon materials for ORR is highly desired because ternary-doping could offer more defective sites and lead to preferable synergistic coupling effects of doped atoms [20, 27, 28]. However, most of the present methods for synthesis of ternary-doped carbon materials involve tedious procedure and/or toxic/expensive precursors. Therefore, it is of essential significance to develop efficient method for green synthesis of ternary-doped CNMs for ORR in both fundamental research and practical applications.

Herein, a P, S, and N ternary-doped graphene, abbreviated as PSNG, was fabricated by a one-step pyrolysis method, in which phosphoric acid was employed as the mild phosphorus source, and thiourea as nitrogen and sulfur sources. The PSNG, as a metal-free catalyst, exhibited a favorable activity for ORR in an alkaline medium comparable with Pt/C. In addition, our proposed catalyst possessed superior stability, making it a promising ORR catalyst for applications in fuel cells and metal-air batteries.

2. Experimental

2.1. Synthesis of heteroatom-doped RGO

GO was synthesized from graphite powder by a modified Hummers' method [27]. For synthesis of P, S and N ternary-doped graphene (PSNG) samples, thiourea was

used as the precursor of N and S, and phosphoric acid (H_3PO_4) as the P doping source. In a typical synthesis of PSNG, 200 mg of graphene oxide was dispersed into 50 mL of 0.1 M phosphoric acid by ultrasonic vibration for 2 h at a concentration of 4.0 mg mL^{-1}. Then, a certain amount of thiourea was added into the above dispersion with vigorously stirring at room temperature for 6 h. The dispersions with different mass ratios of phosphoric acid to thiourea (1:5, 1:10, 1:20) were prepared by varying the weight of thiourea, while keeping the weight of phosphoric acid fixed at 49 mg. The solvent in the mixture was removed in an evaporator operated at 60 $^{\circ}C$ and 300 mbar. The paste mixture obtained was then dried overnight in an oven at 60 $^{\circ}C$. Remnant solid was grinded and pyrolyzed at 900 $^{\circ}C$ in tubular furnace (OTF-1200 MTI Corporation) for 1 h at the ramp rate of 10 $^{\circ}C$ min^{-1} in an Ar_2 atmosphere. When the mass ratios of phosphoric acid to thiourea are 1:5, 1:10 and 1:20, the obtained PSNG samples are termed as PSNG1:5, PSNG1:10 and PSNG1:20, respectively. For comparison, N-doped graphene (NG), or P and N co-doped graphene (PNG) was also prepared through the same steps as those used to make PSNG by adding urea as nitrogen source or using urea and phosphoric acid as nitrogen and phosphorus sources.

2.2 Physical characterizations

The structure of the as-prepared samples was observed under transmission electron microscope (TEM, JEOL-2010 transmission electron microscope operating at 200 kV) and X-ray diffractometer (RIGAK, D/MAX2550 VB/PC, Japan). Field emission scanning electron microscope (FESEM) imaging was performed using a JEOL

JSM-6700F scanning electron microscope. SEM energy-dispersive X-ray (EDX) mapping was performed on a Focused Ion Beam Scanning Electron Microscope (EDS Inca X-Max). Raman spectra were taken on a TriVistaTM555CRS Raman spectrometer at 785 nm. X-ray photoelectron spectroscopy (XPS) analysis was carried out on an ESCLAB 250 spectrometer with a monochromatized Al Kα X-ray source (1486.6 eV photons) to identify surface chemical composition and the bonding state.

2.3 Electrochemical measurements

1 mg of as-prepared PSNG electrocatalyst was immersed in 1 mL of ethanol followed by ultrasonicating for 45 min. To prepare the modified electrode, 55 μL of the catalyst ink was dropped onto the glassy carbon electrode and dried in ambient temperature, resulting in a catalyst loading of 280 μg cm^{-2}. For comparison, the same amount of N-doped graphene, P and N co-doped graphene, or Pt/C (20 wt %) catalyst was also loaded onto the GC electrode with the same procedure.

Rotating disk electrode (RDE) measurements were performed on a CHI660E electrochemical workstation (CH Instruments, USA) in a conventional three-electrode cell using the coated GC electrode (5 mm in diameter) as the working electrode, a platinum wire as the auxiliary electrode, and a saturated calomel electrode (SCE) as the reference electrode. RDE measurements were performed in an O_2-saturated KOH solution at a scan rate of 10 mV s^{-1}. Linear sweep voltammetry measurements were performed at a GC rotating disk electrode with a 5 mm diameter. The rotating ring disk electrode (RRDE) experiments were performed using a Pine Instrument Company AF-MSRCE modulator speed rotator on a CHI660E electrochemical

workstation (CH Instruments, USA). For RRDE experiments, the working electrode was a glassy carbon disk (5.61 mm diameter) and a platinum ring, resulting in a collection efficiency of the ring disk electrode, N = 37 %. These experiments were performed at 1600 rpm with a scan rate of 10 mV s^{-1} in an O_2-saturated KOH solution. The Pt ring electrode was polarized at 0.1 V vs. SCE for oxidizing hydrogen peroxide generated during oxygen reduction at the modified GC disk electrode. During the test, the trachea was put on the solution surface. All electrochemical measurements were carried out at room temperature and performed 3 times to avoid any incidental error.

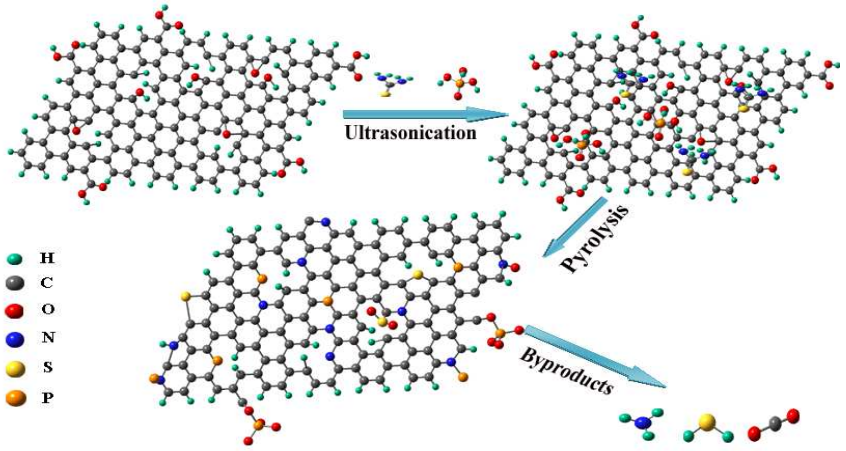

Scheme 1 The synthesis routes of PSNG.

3. Results and discussion

3.1. Characterization of the heteroatom-doped graphene

The obtained PSNG1:10 sample was firstly characterized by TEM and XRD techniques. The TEM image of PSNG1:10 exhibits a wrinkle laminar structure (Fig. 1a), which is similar to previous report on reduced graphene oxide [30]. The partially crinkled nature could originate from the defective structures formed during heteroatoms-doping process [31]. The high-resolution transmission electron

microscope (HRTEM) image and selected area electron diffraction (SAED) pattern confirm the crystalline structure of PSNG1:10 (Fig. 1b). The interlayer spacings of graphitic layers are revealed to be ca. 0.34 nm, which is consistent with the separation of (002) layers of hexagonal graphite [32]. The XRD pattern of PSNG1:10 presents a broad peak at ~26.4 º (Fig.1c) corresponding to an inter-layer spacing of 0.340 nm, which is close to 0.335 nm for graphite and similar to that of the HRTEM result.

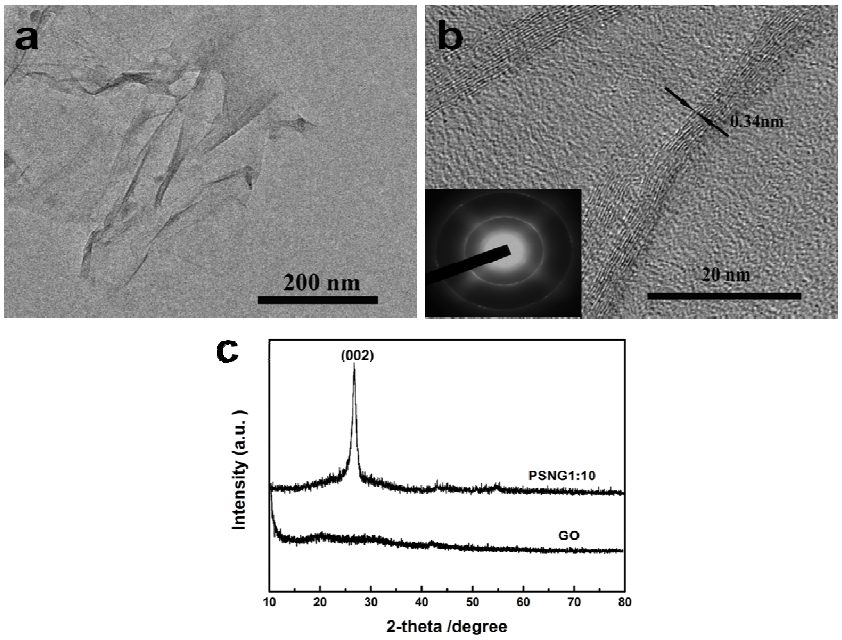

Fig.1 (a) TEM image of PSNG1:10; (b) HRTEM image of PSNG1:10, inset shows the corresponding SAED pattern; (c) XRD patterns of PSNG1:10 and GO.

Fig. 2 shows the FESEM image and corresponding EDX elemental mapping analysis of PSNG1:10. It is revealed that the PSNG1:10 sample is only composed of C, N, O, P and S elements, and the distribution of N, S and P on the graphitic plane is relatively uniform. This fact strongly suggests that the nitrogen, phosphorus and sulfur atoms were doped into the graphene sheets.

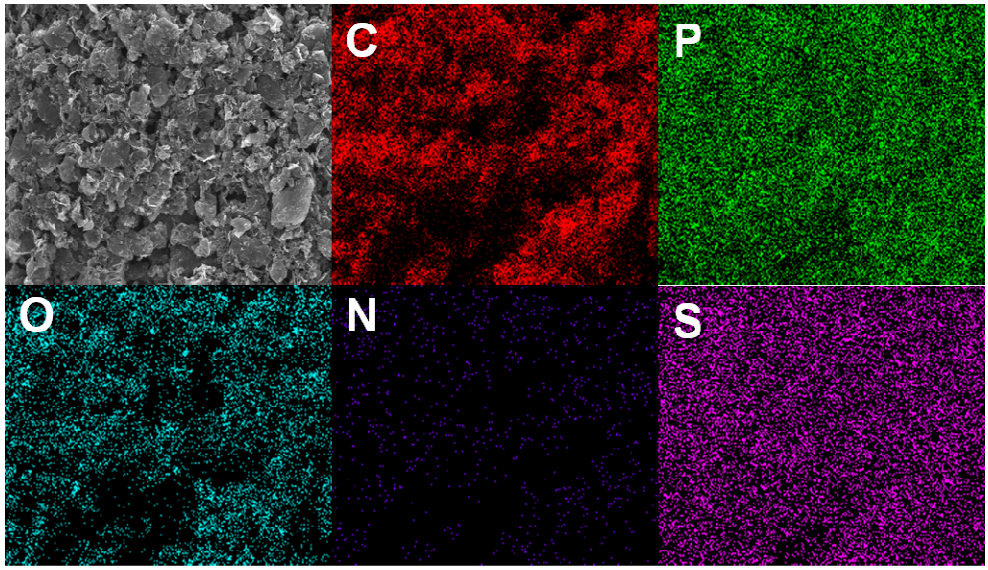

Fig.2 FESEM image and corresponding EDX elemental mappings of PSNG1:10.

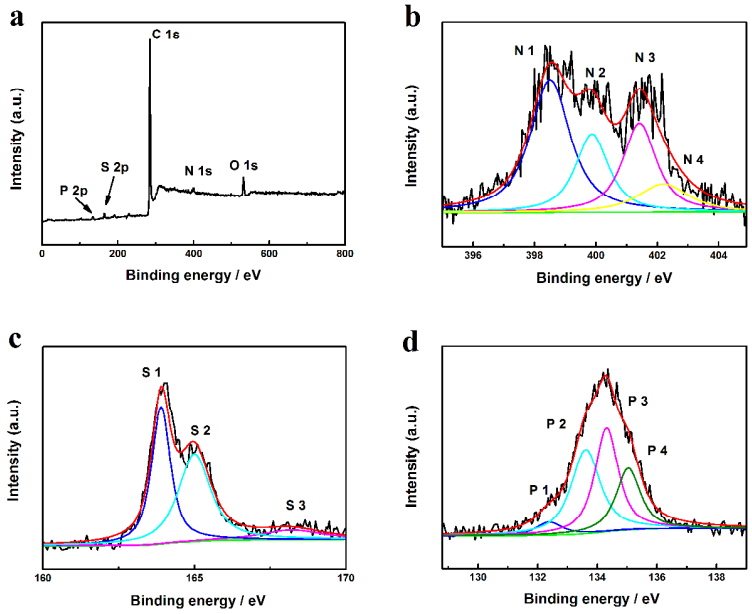

Fig.3 (a) The survey XPS spectra of PSNG1:10. High resolution XPS spectra of (b) N1s, (c) S2p and (d) P2p.

The successful doping of N, P and S into the graphitic matrix of the graphene sheets was further verified by XPS measurements. In Fig. 3a, the full XPS survey spectrum shows the C, N, O, S, and P signals of PSNG1:10, indicating that the N, P,

and S atoms were successfully doped into graphene sheets. The high resolution XPS spectrum can provide more information about the bonding configurations and chemical environments for the doped graphene. As shown in Fig. 3b, the N 1s spectra can be deconvoluted into four different signals with binding energies of 398.3, 399.4, 401.1 and 402.4 eV corresponding to pyridinic N (N1), pyrrolic N (N2), graphitic N (N3) and oxides of nitrogen (N4), respectively [33]. The content of four nitrogen species was listed in Table S1. It can be seen from Table S1, the total content of pyridinic and graphitic N is 66.47% of the doped N atoms in PSNG1:10, which is more than those of other PSNG materials. Previous work demonstrated that these two types of N species act as decisive roles in ORR [34].

We further examined the S2p XPS spectrum, as shown in Fig. 3c.The two peaks at binding energies of around 163.9 and 165 eV can be identified as the spin-orbit coupling positions of 2p3/2 (S1) and 2p1/2 (S2) for thiophene-S, and the third peak at around 168.5 eV corresponds to SOx moieties, which is inoperative for ORR.[35] Thiol group (-SH) signal at around 162 eV was not detected in the S2p XPS spectrum, suggesting that all the sulfur atoms were embedded in the edge and defect of graphene layers in the form of thiophene-S and SOx, without forming thiol groups on the surface of graphene. Table S2 presents the content of thiophene-S and SOx in different samples. It is clear from Table S2 that the content of thiophene-S is nearly invariable for different PSNG samples. It is generally believed that thiophene-S is high-efficient active site for ORR [36].

In Fig. 3d, the high-resolution P2p spectrum reveals that phosphorus was doped

into graphene in four main types of chemical bonding: (P1): P-C (~132.69 eV), (P2): P-N (~133.45 eV), (P3) C-O-PO_3 (~134-134.6 eV) and (P4): metaphosphates (~135.2 eV), respectively [37, 38]. The existence of the P-C covalent bond confirms that phosphorus was successfully doped into the PSNG1:10. The formation of P-N should be due to P-doping in carbon sample containing nitrogen [39]. The existence of P3 indicates that the P was linked to the carbon surface by bonding to one bridging oxygen [40]. P4 should be formed through the condensation of pyrophosphates (or phosphates) [41]. Table S3 gives the content of four phosphorus species. It is seen from Table S3, the PSNG1:10 catalyst possesses the highest content of C-O-PO_3 (36.12%), which is operative for ORR [42].

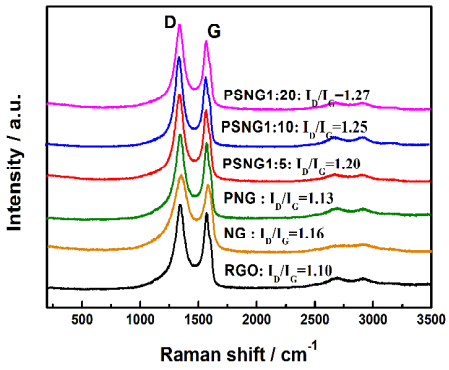

Fig. 4 Raman spectra of RGO, NG, PNG, PSNG1:5, PSNG1:10and PSNG1:20.

To further evaluate the effect of heteroatom doping on graphene, Raman analysis was carried out on virgin graphene oxide as well as doped graphene samples. Fig. 4 shows the comparative Raman spectra of various samples. Raman spectra show that the I_D/I_G ratio increases with the increasing thiourea mass ratio. This can be confirmed from the Raman comparison of NG and PNG with I_D/I_G value of 1.16 and 1.13, respectively, as well as PSNG1:5, PSNG1:10 and PSNG1:20 with I_D/I_G value of 1.20,

1.25 and 1.27, respectively. On the contrary, it can also be seen that the introduction of S into PNG decreases graphitic order, which can be deduced from the difference in I_D/I_G values of PNG and PSNG1:10. This phenomenon should be due to the destruction of the graphitic structure [20].

3.2. Electrocatalytic reduction of oxygen

To investigate the ORR performance, linear sweep voltammetry (LSV) measurements were operated on a rotating disk electrode (RDE) in an O_2-saturated 0.1 M KOH electrolyte. Fig. 5a shows the LSV curves at various rotation speeds for PSNG1:10. Obviously, the diffusion limiting current density increases with increasing rotation speed. To further gain better insight into the electron transfer process for ORR on each sample, the Koutecky-Levich (K-L) plots were obtained for these catalysts at reaction potentials from -0.4 to -0.8 V *vs*. SCE based on LSVs at various rotation speeds (Fig. 5b and Supplementary Fig. S2 b, d, f, g, h and l). The electron transfer number can be calculated from the slope and intercept of the Koutecky−Levich plots, respectively [43]:

$$\frac{1}{J} = \frac{1}{J_K} + \frac{1}{J_L} = \frac{1}{NFKC_0} + \frac{1}{B\omega^{1/2}} \quad (1)$$

$$B = 0.62nFC_0(D_0)^{2/3}\upsilon^{-1/6} \quad (2)$$

Where J is the measured current density, J_K and J_L are the kinetic and diffusion limiting current densities, respectively, n is the overall number of electrons transferred, F is the Faraday constant, C_0 is the bulk concentration of O_2 dissolved in the electrolyte, D_0 is the O_2 diffusion coefficient, v is the kinematic viscosity of the electrolyte, K is the electron transfer rate constant, and ω is the angular velocity of the

disk ($\omega = 2\pi N$, N is the linear rotation speed). The electron transfer number in the O_2 reduction process can be calculated from the slope of the K–L equation.

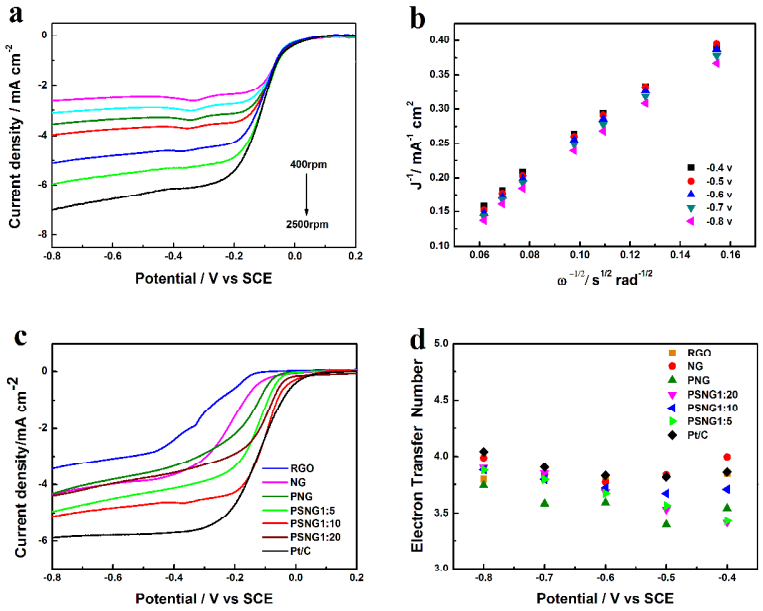

Fig. 5 (a) LSVs of PSNG1:10 for ORR in O_2-saturated 0.1 M KOH under different rotation speeds at a scan rate of 10 mV s^{-1}. (b) The corresponding K-L plots for PSNG1:10 at fixed potentials of -0.4, -0.5, -0.6 -0.7 and -0.8 V vs. SCE, respectively; (c) LSVs of RGO, NG, PNG and PSNG1:5, PSNG 1:10, PSNG 1:20 and Pt/C in O_2-saturated 0.1 M KOH at a scan rate of 10 mV s^{-1} with a rotation speed of 1600 rpm; (d) Electron transfer number of RGO, NG, PNG and PSNG1:5, PSNG1:10, PSNG1:20 and Pt/C at fixed potentials of -0.4, -0.5, -0.6 -0.7 and -0.8 V vs. SCE.

Fig. 5c shows the ORR polarization curves of RGO, NG, PNG, PSNG1:5, PSNG1:10, PSNG1:20 and commercial Pt/C at a rotation speed of 1600 rpm. Tafel plots of LSVs are derived and presented in Supplementary Fig. S2. To evaluate the catalytic efficiency comprehensively, the electrochemical parameters for ORR on these catalysts, including the onset potential (E_{onset}), have-wave potential ($E_{1/2}$),

limiting current density (j_L) and Tafel plot slopes, are compared according to the polarization curves, as seen in Table 1.

Table 1 Electrochemical parameters for ORR estimated from RDE polarization curves in 0.1 M KOH solution.

Catalysts	E_{onset} V *vs.* SCE	$E_{1/2}$ V *vs*. SCE	j_L (mA cm^{-2}) at -0.7 V *vs*. SCE	Tafel plot slopes (mV dec^{-1})
RGO	-0.120	-0.319	3.25	121
NG	-0.064	-0.234	4.13	89
PNG	-0.038	-0.196	4.03	86
PSNG1:5	-0.025	-0.147	4.70	82
PSNG1:10	-0.007	-0.109	4.94	73
PSNG1:20	-0.010	-0.120	4.18	81
Pt/C	0.045	-0.124	5.82	62

Obtained from Fig.7c.

It can be seen from Table 1, the catalytic activity of the ORR on the PSNG1:10 catalyst is apparently better than those on other PSNG materials. The activity enhancement of the PSNG1:10 should be related to more active heteroatom species. XPS results indicate that the content of thiophene-S is nearly unchanged for different PSNG samples. Compared with PSNG1:5 and PSNG1:20 catalysts, however, the PSNG1:10 catalyst possesses dominating active nitrogen (pyridinic-N and graphitic-N) and phosphorus (C-O-PO_3) species, which are high-efficient reactive sites for ORR [17,34,36,42], thus leading to higher catalytic activity of the PSNG1:10 catalyst.

Furthermore, the catalytic activity of PSNG1:10 is also higher than that of RGO, NG, PNG, which should be due to the synergistic coupling between N, S and P. More importantly, the onset potential of PSNG1:10 (-0.007 V) is comparable with that of Pt/C (0.045 V), while the half-wave potential of O_2 reduction on the PSNG1:10 catalyst is even more positive than that of Pt/C, testifying superior activity of our PSNG 1:10 catalyst. The excellent ORR activity of the PSNG 1:10 catalyst is also inferred from the much smaller Tafel slope of 73 mV dec^{-1} in the low overpotential region than those measured with NG, PNG and other PSNG catalysts. The Tafel slope of 73 mV dec^{-1} is close to that of Pt/C (62 mV dec^{-1}), which suggests that the ORR on these two catalysts has a similar catalytic mechanism [44].

The electrocatalytic properties of our PSNG1:10 catalyst are also compared with those previously reported in literature (Table S4). It is worth noting that the onset potential and limiting current density of our catalyst is comparable to or even better than those of previous reports (as shown in Table S4).

Fig. 5d presents the number of electrons transferred at different potentials in the ORR process for all the samples. The electron transfer number (*n*) for ORR on PSNG1:10 varies between 3.76 and 3.97 at applied potentials, suggesting that the PSNG1:10 hybrid favors a 4-electron process for ORR and the final reduced product is almost H_2O. The electron transfer number of Pt/C is determined to be 3.93, agreeing well with the previous report [45].

An additional rotating ring disk electrode (RRDE) experiment can be applied to estimate *n* and further verify the ORR pathways, in which peroxide species produced

during the ORR process at the disk electrode can be detected by the ring electrode. The electron transfer number and the percentage of hydrogen peroxide species can be determined by the following equations [46, 47]:

$$n = \frac{4I_D}{I_D + I_R / N} \qquad (3)$$

$$\%HO_2^- = \frac{200 \times I_R / N}{I_D + I_R / N} \qquad (4)$$

Where I_D is the disk current, I_R is the ring current, and N is the current collection efficiency of the Pt ring.

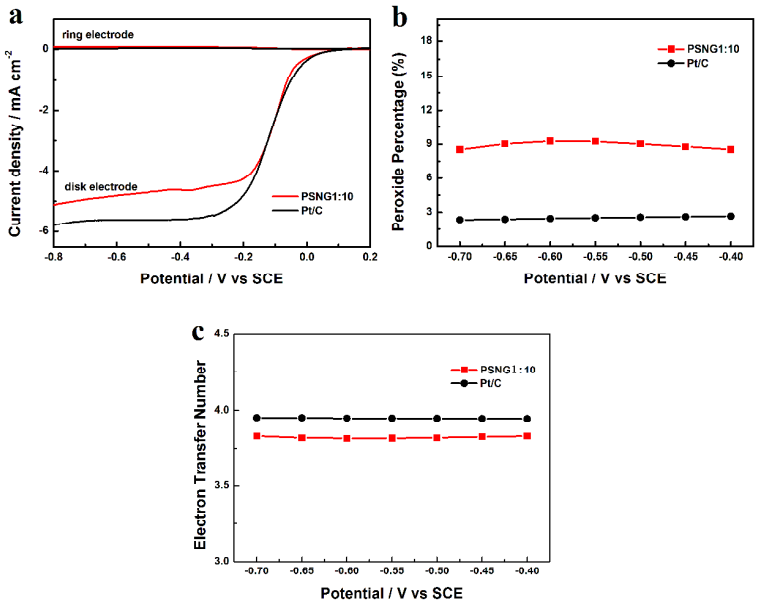

Fig. 6 (a) Rotating ring disk electrode (RRDE) linear sweep voltammograms of PSNG1:10 and Pt/C in O_2-saturated 0.1 M KOH at a scan rate of 10 mV s-1with a rotation speed of 1600 rpm; (b) Peroxide percentage and (c) electron transfer number of PSN1:10 and Pt/C at fixed potentials of -0.4, -0.5, -0.6 and -0.7 V vs. SCE.

Fig. 6a shows the disk current and ring current for the PSNG1:10 and Pt/C catalysts in an O_2-saturated 0.1 M KOH solution. As shown in Fig. 6b, notably, the

measured H_2O_2 yield for PSNG 1:10 is below 10% over the potential range from -0.4 to -0.7 V vs. SCE, and the electron transfer number calculated is in the range of 3.81 to 3.82, which is in accordance with the results calculated from K-L equation, proving high efficiency of the ORR on PSNG 1:10.

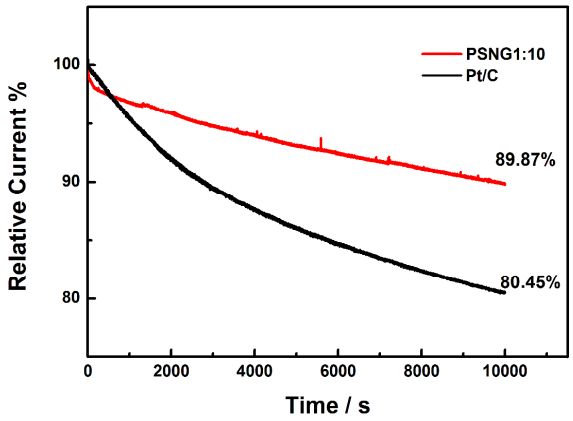

Fig. 7 Stability evaluation of PSNG1:10 and Pt/C for 10000 s in an O_2-saturated 0.1 M KOH solution at -0.3 V vs. SCE with a rotation speed of 1600 rpm.

In addition, the stability for PSNG1:10 and Pt/C was evaluated by current-time chronoamperometric measurements with constant potential set at -0.3 V *vs*. SCE and a rotation speed of 1600 rpm in 0.1 M KOH solution saturated with O_2. Fig. 7 gives the stability test results for PSNG1:10 and Pt/C. The current attenuation loss on Pt/C catalyst is around 13.37 % after a chronoamperometric tests for 10000 s, while PSNG1:10 retains 89.93 % of its initial current under the same conditions. The results demonstrate that the PSNG1:10 catalyst possesses better stability than Pt/C.

4. Conclusion

In summary, this work reports the preparation of a novel ternary-doped graphene catalyst for ORR. Compared with NG and PNG, the obtained PSNG1:10 catalyst for

ORR exhibited higher catalytic activity in terms of more positive onset potential and half-wave potential, and larger diffusion limiting current density, which should be ascribed to the synergetic effect between N, S and P. Furthermore, The PSNG1:10 catalyst also showed better stability than Pt/C. It is believed that the simple but efficient method could be further developed for the production of metal-free electrocatalyst to replace Pt/C in the fields of fuel cells and metal-air batteries in the future.

Acknowledgements

This research has been financed by the National Natural Science Foundation of China (No. 21273024), Natural Science Foundation of Jilin Province, China (No. 201215135) and Scientific Research Foundation of the Education Department of Jilin Province, China (No. KYC-JC-XM-2013-021).

References

[1] H. A. Gasteiger and N. M. Marković, *Science*, 2009, **324**, 48-49.

[2] M. Prabu, K. Ketpang and S. Shanmugam, *Nanoscale*, 2014, **6**, 3173-3181.

[3] M. H. Huang, Y. D. Jin, H. Q. Jiang, X. P. Sun, H. J. Chen, B. F. Liu, E. K. Wang, S. J. Dong, *J. Phys. Chem. B*, 2005, **109**, 15264-15271.

[4] L. P. Zhang, Z. H. Xia, *J. Phys. Chem. C*, 2011, **115**, 11170-11176.

[5] J. R. C. Salgado, E. Antolini, E. R. Gonzalez, *J. Power Sources*, 2004, **138**, 1-2.

[6] Z. S. Wu, S.B. Yang, Y. Sun, K. Parvez, X. L. Feng, K. Mullen, *J. Am. Chem. Soc.*, 2012, **134**, 9082-9085.

[7] M. S. Ahmed, S. Jeon, *J. Electrochem. Soc.*, 2014, **161**, F1300-F1306.

[8] S. N. S. Goubert-Renaudin, X. L. Zhu, A. Wieckowski, *Electrochem. Commun.*, 2010,**12**, 1457-1461.

[9] L. J. Yang, S. J. Jiang, Y. Zhao, L. Zhu, S. Chen, X. Z. Wang, Q. Wu, J. Ma, Y. W. Ma, Z. Hu, *Angew. Chem. Int. Ed.*, 2011, **50**, 7132-7135.

[10] U. B. Nasini, V. G. Bairi, S. K. Ramasahayam, S. E. Bourdo, T. Viswanathan, A.U. Shaikh, *J. Power Sources*, 2014, **250**, 257-265.

[11] J. Xu, Y. Zhao, C. Shen, L. Guan, *ACS Appl. Mater. Interfaces*, 2013, **5**, 12594-12601.

[12] L. Liao, H. Peng, Z. Liu, Chemistry makes graphene beyond graphene, *J. Am. Chem. Soc.*, 2014, **136**, 12194-12200.

[13] E. Yoo, H. Zhou, *ACS Nano*, 2011, **5**, 3020-3026.

[14] K. Gong, F. Du, Z. Xia, M. Durstock, L. Dai, *Science*, 2009, **323**, 760-764.

[15] S. Wang, L. Zhang, Z. Xia, A. Roy, D. W. Chang, J.B. Baek, L. Dai, *Angew. Chem. Int. Ed. Engl.*, 2012, **51**, 4209-4212.

[16] D. S. Geng, N. Ding, T. S. Andy Hor, Z. L. Liu, X. L. Sun and Y. Zong, *J. Mater. Chem. A*, 2015, **3**, 1795- 1810

[17] D. S. Geng, Y. Chen, Y. G. Chen, Y. L. Li, R. Y. Li, X. L. Sun, S. Y. Yeb, S. Knights, *Energy Environ. Sci*. 2011, **4**, 760-764.

[18] Y. Liu, S. Chen, X. Quan, H. Yu, H. Zhao, Y. Zhang, G. Chen, *J. Phys. Chem. C,* 2013,**117** ,14992-14998.

[19] C. H. Choi, M. W. Chung, H. C. Kwon, S. H. Parka, S. I. Woo, B, *J. Mater. Chem. A*, 2013, **1**, 3694-3699.

[20] F. Razmjooei, K. P. Singh, M.Y. Song, J. S. Yu, *Carbon*, 2014, **78**, 257-267.

[21] Y. Chang, F. Hong, C. He, Q. Zhang, J. Liu, *Adv. Mater.*, 2013, **25**, 4794-4799.

[22] J. Liu , X. J. Sun , P. Song , Y. W. Zhang , W. Xing and W. L. Xu, *Adv. Mater.*, 2013, **25**, 6879-6883.

[23] L. Zhang, J. Niu, M. Li, Z. Xia, *J. Phys. Chem. C,* 2014, **118,** 3545-3553.

[24] B. Zhang, Z. Wen, S. Ci, S. Mao, J. Chen, Z. He, *ACS Appl. Mater. Interfaces*, 2014, **6**, 7464-7470.

[25] D. Shin, B. Jeong, B. S. Mun, H. Jeon, H.-J. Shin, J. Baik, J. Lee, *J. Phys. Chem. C*, 2013, **117**, 11619-11624.

[26] P. Chen, T. Y. Xiao, Y. H. Qian, S. S. Li, S.H. Yu, *Adv. Mater.*, 2013, **25**, 3192-3196.

[27] S. Dou, A. Shen, Z. L. Ma, J. H. Wu, L. Tao, S. Y. Wang, doi:10.1016/j.jelechem.2015.05.013.

[28] S. Y. Zhao, J. Liu, C. X. Li, W. B. Ji, M. M. Yang, H. Huang, Y. Liu, Z. H. Kang, *ACS Appl. Mater. Interfaces,* 2014, **6**, 22297-22304

[29] Z. Chen, D. Higgins and Z. W. Chen, *Carbon*, 2010, **48**, 3057-3065.

[30] W. Gao, L. B. Alemany, L. J. Ci, P. M. Ajayan, *Nat. Chem.*, 2009 , **1**,403-408.

[31] S. B. Yang, L. J. Zhi, K. Tang, X. L. Feng, J. Maier, K. Mullen, *Adv. Funct. Mater.*, 2012, **22**, 3634-3640.

[32] H. B. Li, W. J. Kang, L. Wang, Q. L. Yue, S. L. Xu, H. S. Wang, J. F. Liu, *Carbon*, 2013, **54**, 249-257.

[33]W. Ding, Z. Wei, S. Chen, X. Qi, T. Yang, J. Hu, D. Wang, L. J. Wan, S. F. Alvi,

L. Li, *Angew. Chem. Int. Ed Engl.*, 2013, **52,** 11755-11759.

[34] H. Kim, K. Lee, S.I. Woo, Y. Jung, *Phys. Chem. Chem. Phys.*, 2011, **13,** 17505-17510.

[35] Z. Yang, Z. Yao, G. F. Li, G. Y. Fang, H. G. Nie, Z. Liu, X. M. Zhou , X. A. Chenand,S. M. Huang, *ACS Nano.*, 2012, **6**, 205-211.

[36] J. E. Park, Y. J. Jang, Y. J. Kim, M. S. Song, S. Yoon and D. H. Kim, *Phys.Chem.Chem. Phys.*, 2014, **16**, 103-109.

[37] Y. Zhang, T. Mori, J. Ye, M. Antonietti, *J Am Chem. Soc.*, 2010,**132**, 6294-6295.

[38] C. Wang, L. Sun, Y. Zhou, P. Wan, X. Zhang, J. Qiu, *Carbon*, 2013, **59**, 537-546.

[39] J. M. Rosas, R. R. Rosas, J. R. Mirasol, T. Cordero, *Carbon*, 2012, **50**, 1523-1537.

[40] X. Wu, L. R. Radovic, *Carbon*, 2006, **44**, 141-151.

[41] C. Wang, L. Sun, Y. Zhou, P. Wan , X. Zhang, J. Qiu , *Carbon*, 2013, **59**, 537-646.

[42] C. H. Choi, S. H. Park ,S. I. Woo, *ACS Nano*, 2012, **6**, 7084-7091.

[43] Z. W. Xu, H. J. Li, G. X. Cao, Q. L. Zhang, K. Z. Li and X. N. Zhao, *J. Mol. Catal. A: Chem.*, 2011, **335**, 89-96.

[44] S. K. Bikkarolla, F.J. Yu, W.Z. Zhou, P. Joseph, P. Cumpson and P. Papakonstantinou, *J. Mater. Chem*. *A*, 2014, **2**, 14493-14501.

[45] S. Jiang, C. Z. Zhou, S. J. Dong, *J. Mater. Chem. A*, 2013, **1**, 3593-3599.

[46] J. Masa, W. Schuhmann, *Chem. Eur. J.*, 2013, **19**, 9644-9654.

[47] T. S. Olson, S. Pylypenko, J. E. Fulghum and P. Atanassov, *J. Electrochem. Soc.*, 2010, **157**, B54-B63.